ACS OMEGA

http://pubs.acs.org/journal/acsodf

Article

Substituent-Controlled Structural, Supramolecular, and Cytotoxic Properties of a Series of 2-Styryl-8-nitro and 2-Styryl-8-hydroxy Quinolines

Suman Sehlangia, Namyashree Nayak, Neha Garg,* and Chullikkattil P. Pradeep*

Cite This: *ACS Omega* 2022, 7, 24838−24850

Read Online

ACCESS | Metrics & More | Article Recommendations | Supporting Information

ABSTRACT: Styryl quinolines are biologically active compounds with properties largely depending on the substituents on the styryl and quinoline rings. The supramolecular aspects of this class of compounds are rarely explored. In this study, two new series of styryl quinoline derivatives, bearing −OH and $-NO_2$ groups at the eighthposition of the quinoline ring and $-SCH_3$, $-OCH_3$, and −Br groups on the styryl ring, have been developed, and their structural, supramolecular, and cytotoxic properties have been analyzed. Crystallographic analyses revealed the exciting substituent-dependent structural and supramolecular features of these compounds. In general, the 8 −OH substituted derivatives (**SA** series) exhibited a non-planar molecular geometry having larger dihedral angles (5.75−59.3°) between the planes of the aromatic rings. At the same time, the 8 $-NO_2$ substituted derivatives (**SB** series) exhibited a more or less planar molecular geometry, as revealed by the smaller dihedral angles (1.32−3.45°) between the aromatic rings. Multiple O−H···O, C−H···O, O−H···N, and $\pi-\pi$ stacking interactions among the molecules lead to fascinating supramolecular architectures such as hydrogen-bonded triple helices, zig-zag 1D chains, $\pi-\pi$ stacked infinite chains, and so forth in their crystal lattice. Hirshfeld surface analyses confirmed the existence of strong $\pi-\pi$ stacking and other weak bonding interactions in these compounds. The preliminary cytotoxic properties of **SA** and **SB** series compounds were evaluated against the human cervical cancer cell lines (HeLa cells), which further highlighted the roles of functional substituents on the aromatic rings. The **SA** series compounds with the −OH substituent on the quinoline ring exhibited better cytotoxicity than the **SB** series compounds with a $-NO_2$ substituent. Similarly, the electron-withdrawing group −Br on the styryl ring enhanced the cytotoxicity in both series. The IC_{50} values were 2.52−4.69 and 2.897−10.37 μM, respectively, for the **SA** and **SB** series compounds. Compound **S3A** having −OH and −Br groups on the quinoline and styryl ring, respectively, exhibited the best IC_{50} value of 2.52 μM among all the compounds tested. These findings confirm the relevance of the hydroxyl group in the eighth position of quinoline. In short, the present study attempts to provide a systematic analysis of the effects of aromatic ring substituents on the structural, supramolecular, and cytotoxic properties of styryl quinolines for the first time.

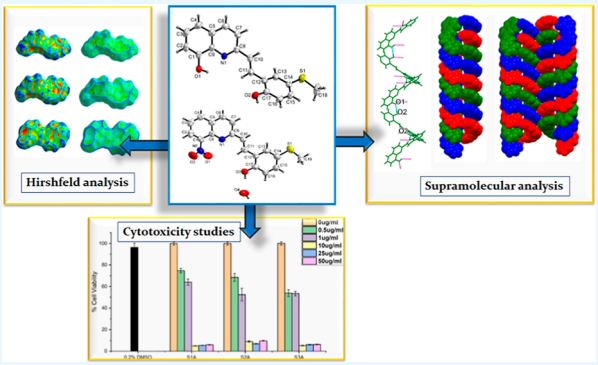

1. INTRODUCTION

8-Hydroxyquinolines (8-HQs) belong to the quinoline family of heterocycles and are known for their pharmacological, optical, and analytical applications. The core structure of 8-HQs, consisting of fused pyridine and phenol rings, is considered a privileged structure for developing novel drug molecules and materials.[1,2] The synthetic versatility of 8-HQs allows the generation of targeted derivatives with fine-tuned properties for a broad spectrum of applications. The interlinking of the 8-HQs with a phenyl ring through an unsaturated ethylene linker leads to 2-styryl-8-hydroxyquinolines (2S-8HQs), a highly useful derivative of 8-HQs. Such interlinking helps extend the π-conjugation of 8-HQs, enhancing the molecule's overall electron mobility, thermal stability, and lipophilicity. As a result, the 2S-8HQs exhibit improved photophysical, conductive, and biological properties compared to simple 8-HQs.[3−10] By introducing suitable functional substituents on the styryl and quinoline rings, the properties of 2S-8HQs can be improved. 2S-8HQs exhibit important pharmacological activities, including anticancer, anti-HIV-1, antimicrobial, antimalarial, and anti-Alzheimer activities.[11−21] In addition, the 2S-8HQs are also explored as organic semiconductors,[22−24] thermo and electrochromic materials,[25] and organic light-emitting diode (OLED) materials.[22,23,26−28] Still, compared to many other derivatives

Received: May 16, 2022
Accepted: June 28, 2022
Published: July 8, 2022

of 8-HQs, 2S-8HQs are a relatively less explored class of compounds, and there is an ongoing interest in developing structurally diversified 2S-8HQs for varied applications.

The principles of supramolecular chemistry are extensively used in engineering materials for therapeutic, optical, and other diverse applications.[29−32] A single non-covalent interaction may be weak, but a collection of many such interactions can lead to materials with properties resembling the covalently bonded materials. The rational design of molecular systems incorporating structural motifs exhibiting specific and directional molecular recognition properties is vital in developing new materials across disciplines. For example, face-to-face $\pi-\pi$ stacking interactions are beneficial for organic semiconductor applications.[33] Similarly, planar rigid structures with extended conjugation are vital for OLED applications.[34] Most importantly, supramolecular interactions play significant roles in many biological systems and drug molecules. Establishing quinoline derivatives as reliable tectons in supramolecular chemistry is important in this context. However, quinoline is a less explored structural motif in supramolecular chemistry despite its ability to exhibit strong C−H···π and $\pi-\pi$ stacking interactions.[3,26,35,36] The available reports in this direction are mainly on the metal complexes of quinoline derivatives. For example, multinuclear metal complexes,[33,37] coordination polymers,[38,39] and metal−organic frameworks[40] have been reported using 2S-8HQ derivatives as versatile ligands. In these compounds, the 2S-8HQ ligands exhibit multiple weak bonding interactions, including C−H···O, O−H···O, C−H···π, and $\pi-\pi$ stacking interactions, leading to supramolecular architectures such as helices, 3D frameworks, and coordination networks.[10,41−44] These studies show that the supramolecular features of 2S-8HQ-based complexes can be tuned by varying the substituents on the styryl or quinoline rings.

A clear understanding of the structural and supramolecular properties of quinoline derivatives, especially styryl-quinoline derivatives, may help design novel materials for diverse applications. However, only a few structural reports on 2S-8HQs are available,[45,46] and the detailed supramolecular analyses, including Hirshfeld surface analyses,[47,48] are rarely reported for this class of compounds. Moreover, structural studies on the 8 $-NO_2$ analogues of 2S-8HQs are unprecedented. In this paper, a new series of 2S-8HQs (**S1A−S3A**, **SA** series) and the corresponding 8 $-NO_2$ analogues 2-styryl-8-nitro quinolines (2S-8NQs) (**S1B−S3B**, **SB** series) have been developed, and their detailed structural and supramolecular analyses, including Hirshfeld surface analyses, are being reported for the first time, see Scheme 1. Furthermore, preliminary studies on the cytotoxic properties of these new compounds are reported herein. The effects of different substituents on these compounds' structural, supramolecular, and cytotoxic properties have been analyzed.

2. RESULTS AND DISCUSSION

2.1. Design and Synthesis of SA and SB Series Compounds. The **SA** and **SB** series compounds were synthesized by reacting the commercially available quinaldines, 2-methyl quinoline-8-ol, and 2-methyl-8-nitroquinoline, respectively, with substituted aldehydes in acetic anhydride, as shown in Scheme 1. The aldehyde derivatives **E2** and **E3** are available commercially, whereas **E1** was synthesized following a reported procedure.[49] The condensation of quinaldines with the aldehydes yielded the acetylated styryl quinolines **F1−F6**. The acetyl derivatives were hydrolyzed in the presence of

Scheme 1. General Scheme Showing the Synthesis and Chemical Structure of SA and SB Series Compounds Explored in This Study

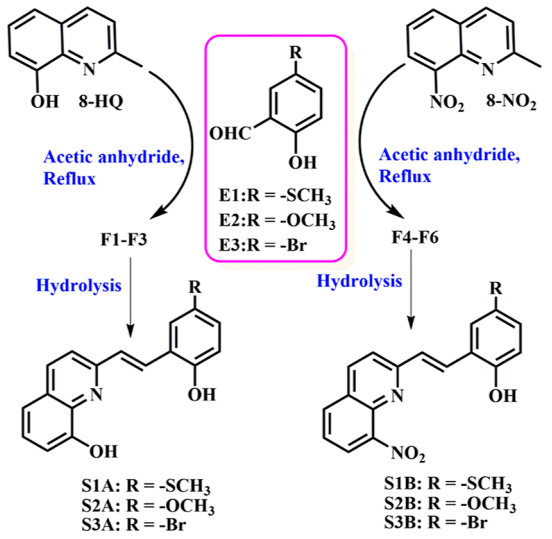

K_2CO_3 and neutralized with HCl to give the final products **S1A−S3A** and **S1B−S3B**.[50] Standard analytical and spectroscopic techniques confirmed the reaction products; see Figures S1−S39 Supporting Information. **S1A−S3A** and **S1B−S3B** exhibited ^{1}H NMR peaks in the range 7.09−8.37 ppm with J values 15.08−16.45 ppm, confirming the presence of *trans* vinylene groups.[46,50,51] The characteristic ^{1}H NMR peaks due to the hydroxyl groups appeared at 9.57−10.60 ppm. Single-crystal X-ray diffraction analyses were performed for the final characterization of these compounds. Suitable single crystals of these compounds were grown from the methanol/dichloromethane solvent mixture by slow evaporation.

2.2. Structural Analyses of the SA Series Compounds. The structure refinement data of **S1A−S3A** are given in Table S1 (Supporting Information), and the molecular structures showing the atom labeling scheme are presented in Figures 1a,b and 3a, respectively. These compounds crystallized in the monoclinic $P2_1/n$ space group with a single molecule in the asymmetric unit. The crystal structure analyses confirmed that these compounds show E conformation about the styryl C=C bond. **S1A** and **S2A** exhibited a non-planar, twisted molecular geometry evident from their dihedral angles of 59.3 and 47.07°, respectively, between the planes of the quinoline and styryl rings. In comparison, **S3A** showed a planar geometry with a smaller dihedral angle of 5.75° between the planes of the quinoline and styryl rings. **S1A−S3A** exhibited typical styryl alkenyl bond lengths of 1.320(3), 1.328(4), and 1.322(4) Å, respectively.[3]

The crystallographic analyses revealed that **S1A** and **S2A** exhibit similar supramolecular features. Both these compounds show two prominent O−H···O intermolecular interactions (O1−H1···O2 and O2−H2···O1) between the −OH groups on the quinoline and styryl moieties of adjacent molecules; see Table S3, Supporting Information for details. These interactions proceed in a helical fashion along the crystallographic b axis, as shown in Figures 2a and S40a. In the crystal lattice of **S1A** and **S2A**, three such supramolecular helices are arranged concentrically along the b axis, Figures 2b and S40b. As there are three concentric helices along the b axis, the unit cell parameter b is one-third of the pitch of the helical chains,

https://doi.org/10.1021/acsomega.2c03047
ACS Omega 2022, 7, 24838−24850

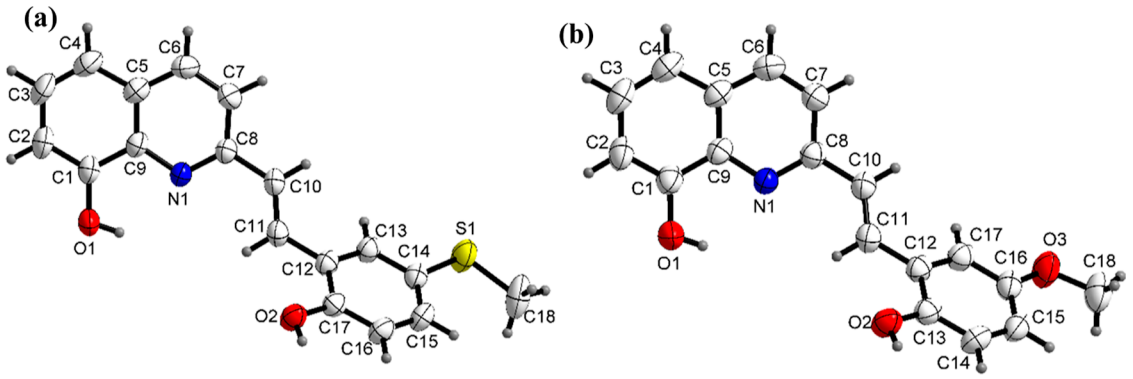

Figure 1. Molecular structures of (a) **S1A** and (b) **S2A** showing the atom labeling scheme; thermal ellipsoids are shown at the 50% probability level.

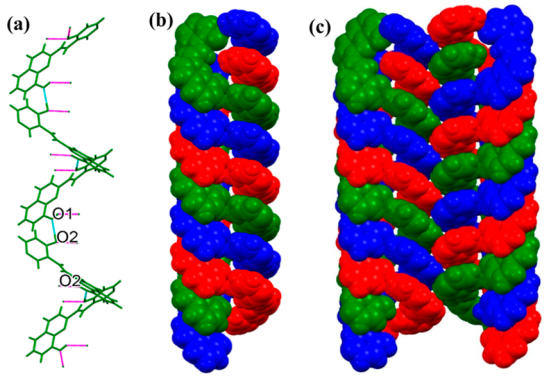

Figure 2. (a) Depiction of various H-bonding interactions exhibited by **S1A**; (b) the formation of supramolecular H-bonded helices in the crystal lattice of **S1A**; (c) the left- and right-handed triple helices are arranged in a rare "ridges-in-groves" fashion in the crystal lattice of **S1A**. H-bonding interactions are shown in turquoise, and hanging contacts are shown in pink.

that is, 5.1317(2) Å. Each helical chain is connected to the other two helical chains through two O−H···O interactions. The quinoline phenolic oxygen O1 acts as the H-bond donor in one of these interactions, while the styryl phenolic oxygen O2 acts as the acceptor in the other. The arrangement of the helical chains in a concentric fashion is supported by $\pi-\pi$ stacking interactions between the quinoline rings; see Table S4 and Scheme S1 in the Supporting Information for details. Here, we have considered only strong $\pi-\pi$ stacking interactions that are characterized by short centroid−centroid distances (~3.8 Å), near-parallel ring planes (α < 10 to ~0°), and small slip angles (β, γ < 25°) and vertical displacements (slippage < 1.5 Å). In these interactions, the quinoline moieties of adjacent molecules are stacked in an offset fashion such that the pyridine ring of one molecule is on top of the phenyl ring of the second. In the case of **S1A**, the perpendicular distance between the rings is in the range 3.57−3.62 Å, and the dihedral angles between the planes of the rings, that is, α, is 2.34° with a slip angle β (formed by centroid−centroid vector and the ring normal) of 18.3−20.5°. However, in **S2A**, the perpendicular distance between the rings is comparatively shorter, that is, 3.46−3.49 Å, with several C−C distances around 3.6 Å. The rings are almost parallel (dihedral angle between the planes α = 1.59°) in an offset arrangement with a slip angle β of 17.6−18.8°.

S1A and **S2A** crystallized in a centrosymmetric space group with the molecules arranged in a centrosymmetric fashion in the unit cell. Furthermore, the crystal lattice contains pairs of

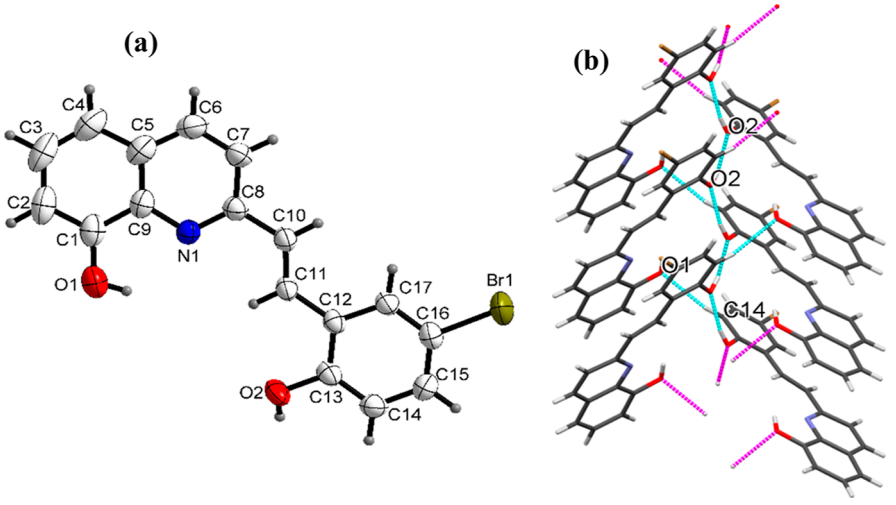

Figure 3. (a) Molecular structure of **S3A** showing atom labeling scheme. Thermal ellipsoids are shown at the 50% probability level; (b) the strong O−H···O intermolecular hydrogen bonding interactions (O2−H2···O2) between the phenolic −OH groups proceed in a 1D chain fashion. H-bonding/weak-bonding interactions are shown in turquoise, and hanging contacts are shown in pink.

https://doi.org/10.1021/acsomega.2c03047
ACS Omega 2022, 7, 24838−24850

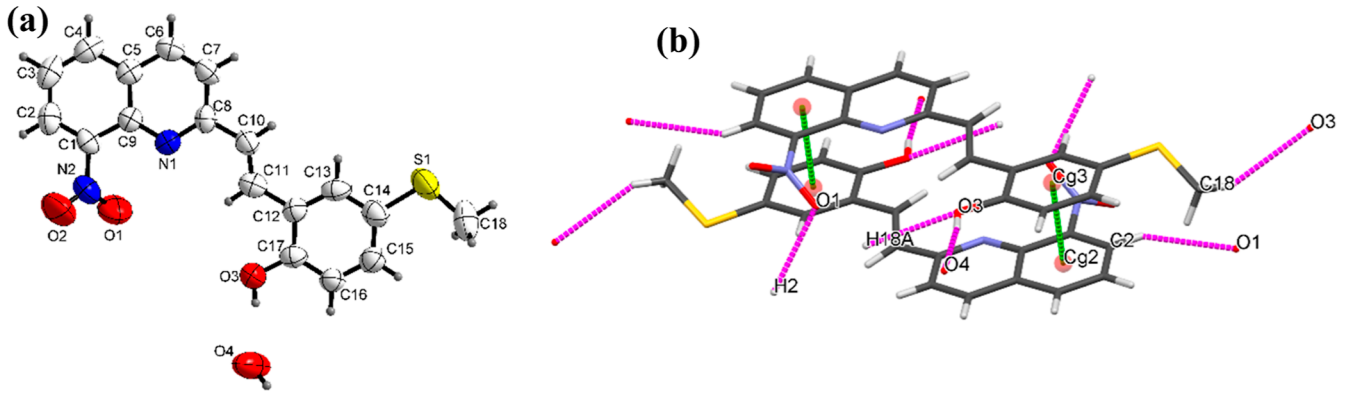

Figure 4. (a) Molecular structure of **S1B** showing atom labeling scheme. Thermal ellipsoids are shown at the 50% probability level; (b) strong $\pi-\pi$ stacking interactions between adjacent molecules of **S1B** (green dotted lines) lead to forming π stacked dimers. Hanging contacts are shown in pink.

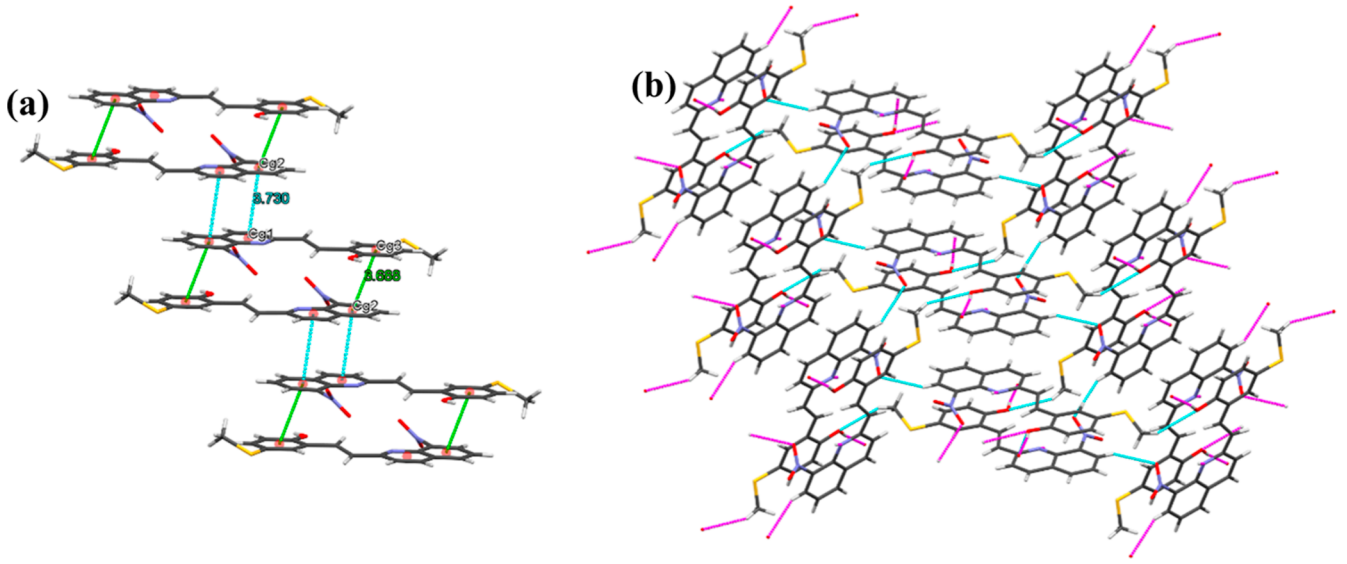

Figure 5. (a) π-Stacked dimers undergo further $\pi-\pi$ stacking interactions (turquoise dotted lines) with other dimers in a stepped fashion leading to infinite chains in the crystal lattice of **S1B**; (b) the adjacent π-stacked chains are arranged in a zig-zag fashion in the crystal lattice. These chains are further interconnected through various H-bonding/weak bonding interactions (turquoise dotted lines) into a 3D network structure. The hanging contacts are shown in pink.

opposite-handed triple-helical chains, as shown in Figures 2c and S40c. Interestingly, it can be seen that these left- and right-handed triple helices are arranged in a rare "ridges-in-groves" fashion in these molecules. This packing mode of opposite-handed triple helices allows for tighter packing and greater intermolecular contacts.[51] Triple helical systems are extremely important in supramolecular chemistry because of their relevance to biological systems such as DNA.[52−56] It was proposed that the triple helices represent the addition of an extra DNA strand to the double-helical structure. Triple helical systems have been actively pursued in recent years because of their significance in medicinal chemistry. We assume that the twisted molecular geometry of **S1A** and **S2A** and their strong supramolecular interactions play vital roles in forming the supramolecular helices in the crystal lattice.

Meanwhile, the crystal packing of **S3A** is dominated by intermolecular O−H···O and C−H···O interactions; see Table S3 in the Supporting Information for details. The O−H···O interactions (O2−H2···O2) between the styryl phenolic −OH groups extend in a zig-zag 1D chainlike fashion along the *b* axis, see Figure 3b. A weak C−H···O interaction (C14−H14···O1) involving a styryl ring carbon (C14) and the −OH group on the quinoline ring also supports the zig-zag 1D chains.

Comparing the structural features of **S1A**−**S3A**, it is noted that the molecules **S1A** and **S2A** have a twisted, non-planar geometry, while **S3A** has a planar geometry. **S1A** and **S2A** possess $-SCH_3$ and $-OCH_3$ groups, respectively, on the styryl ring, while **S3A** bears a −Br unit. It can be noted that the introduction of an electron-withdrawing group (EWG) such as −Br on the styryl phenolic ring makes the molecule more planar compared to the twisted molecular structure exhibited by **S1A** and **S2A**, having electron-donating groups (EDGs) $-SCH_3$ or $-OCH_3$. The difference in the molecular structure, in turn, affects the supramolecular structures as well. The absence of a twisted molecular geometry in **S3A** leads to a zig-zag chainlike arrangement instead of a helical structure. Another observation is that **S1A** and **S2A** exhibit aromatic $\pi-\pi$ stacking interaction among molecules, while **S3A** does not show such interactions. These observations suggest that the nature of the substituents on the styryl ring affects the structural and supramolecular features of 2S-8HQ derivatives.

https://doi.org/10.1021/acsomega.2c03047
ACS Omega 2022, 7, 24838−24850

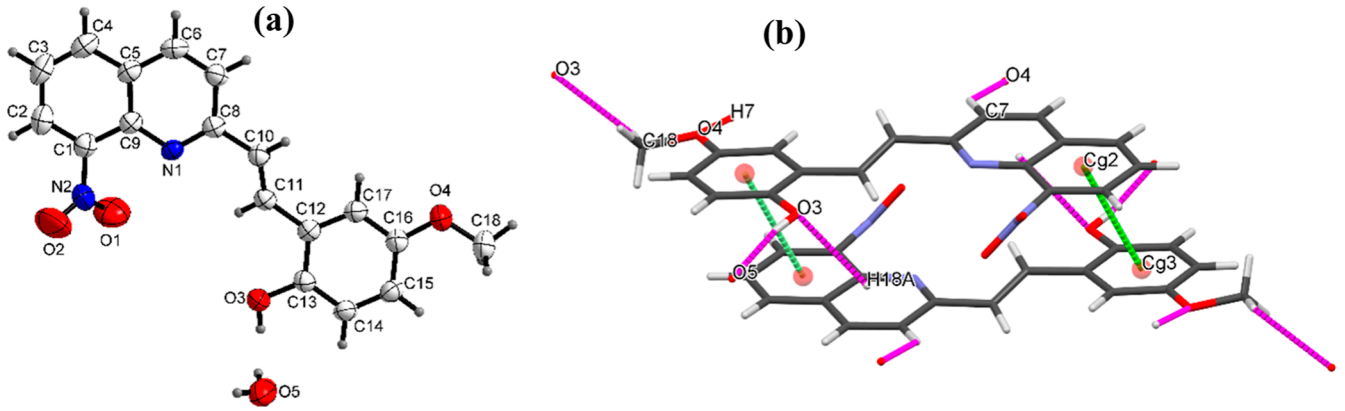

Figure 6. (a) Molecular structure of **S2B** showing the atom labeling scheme. Thermal ellipsoids are shown at a 50% probability level; (b) strong $\pi-\pi$ stacking interactions between adjacent molecules of **S2B** (green dotted lines) lead to the formation of π stacked dimers.

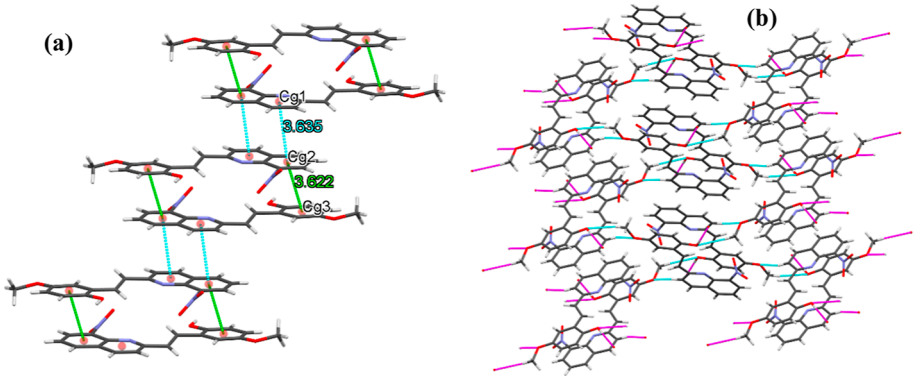

Figure 7. (a) π-Stacked dimers undergo further stacking interactions (turquoise dotted lines) in an offset fashion in **S2B**, leading to infinite chains; (b) the π-stacked chains are further inter-connected through various hydrogen/weak bonding interactions (turquoise dotted lines), leading to a highly hydrogen-bonded 3D network in the crystal lattice. The hanging contacts are shown in pink.

2.3. Structural Analyses of the SB Series Compounds.

Among the **SB** series compounds having a $-NO_2$ substituent at the eighth position of the quinoline ring, **S1B** and **S2B** crystallized in the orthorhombic *Pbca* space group, while **S3B** crystallized in the monoclinic $P2_1/c$ space group. The asymmetric unit contains one molecule of the compound and a solvent water molecule in all these cases. **S1B**–**S3B** showed *E* conformation about the styryl C=C bond; see Figures 4a, 6a, and 8a. The crystallographic data of **S1B**–**S3B** are given in Table S2 in the Supporting Information. One important observation about the structural features of **SB** series compounds is that they exhibit a planar molecular geometry compared to the **SA** series compounds. This is evident from the dihedral angles of 1.32–3.45° shown by the **SB** series compounds between the planes of the aromatic rings. **SB** series compounds also exhibited typical styryl alkenyl bond distances in the range of 1.298(5)–1.326(4) Å.

The molecular structure of **S1B** showing the atom labeling scheme is given in Figure 4a. In the crystal lattice of **S1B**, strong $\pi-\pi$ stacking interactions between the adjacent molecules lead to the formation of π-stacked dimers, as shown in Figure 4b. In these dimers, the molecules are stacked head-to-tail, that is, the styryl phenol ring of one molecule interacts with the quinoline ring of the other and vice versa. The centroid-to-centroid distances are 3.59–3.73 Å, and the perpendicular distances between the rings are 3.42–3.49 Å in these dimers.

In the crystal lattice, such π-stacked dimers undergo further $\pi-\pi$ stacking interactions leading to infinite chains, see Figure 5a. In this inter-dimer stacking, the quinoline rings of the adjacent dimers interact because of which the stacking proceeds in an offset/stepped fashion. The adjacent π-stacked chains are arranged in a zig-zag fashion in the crystal lattice, see Figure 5b. The π-stacked chains are further interlinked into the 3D network structure by several O–H···O and N–H···O intermolecular interactions exhibited by **S1B** molecules, as shown in Figure 5b. The details of the H-bonding interactions are listed in Table S5 in the Supporting Information, and the details of the $\pi-\pi$ stacking interactions are listed in Table S6 in the Supporting Information.

S2B also shows supramolecular interactions quite similar to **S1B**. Solid $\pi-\pi$ stacking interactions between adjacent molecules of **S2B** lead to π-stacked dimers, as shown in Figure 6b. The molecules are arranged in a head-to-tail fashion (styryl to quinoline ring distance 3.622 Å) in these dimers, which undergo further $\pi-\pi$ stacking interactions with adjacent dimers in a stepped fashion forming infinite chains, see Figure 7a. The π-stacked chains are further inter-connected through various hydrogen/weak bonding interactions (C18–H18···O3, C7–H7···O4, and O3–H3···O5, see Figure 6b), leading to a highly hydrogen-bonded 3D network of $\pi-\pi$ stacked dimers in the crystal lattice, Figure 7b.

In the crystal lattice of **S3B**, hydrogen bonding interactions exist between the styryl phenolic –OH and the quinoline N with the solvent water molecules (O3···O4 interaction and

https://doi.org/10.1021/acsomega.2c03047
ACS Omega 2022, 7, 24838–24850

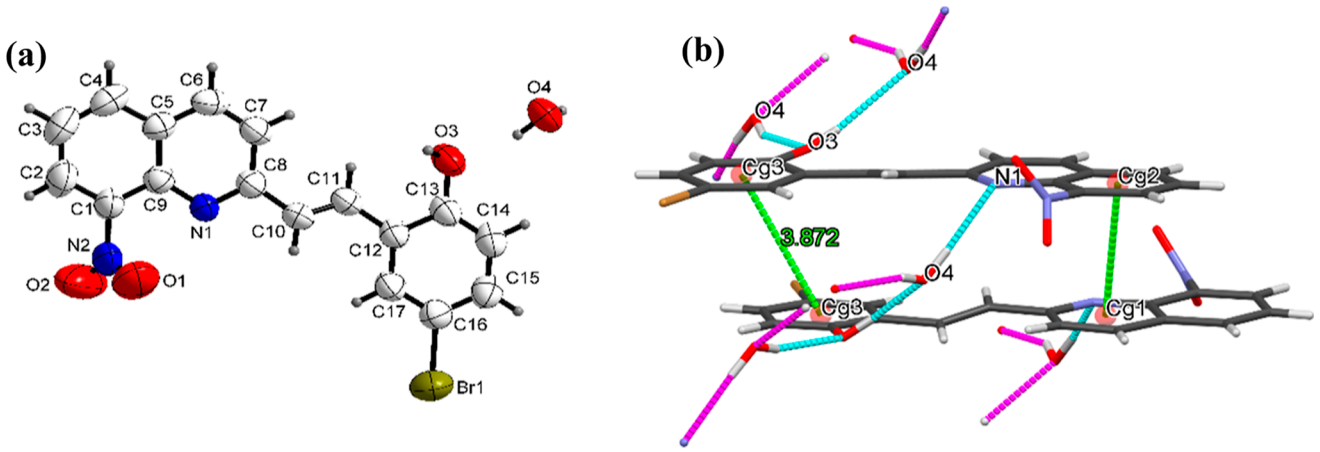

Figure 8. (a) Molecular structure of **S3B** showing the atom labeling scheme. Thermal ellipsoids are shown at a 50% probability level; (b) the O3···O4 and N1···O4 interactions (turquoise dotted lines) and the $\pi-\pi$ stacking interactions (green dotted lines) lead to stacked dimers in **S3B**. Hanging contacts are shown in pink.

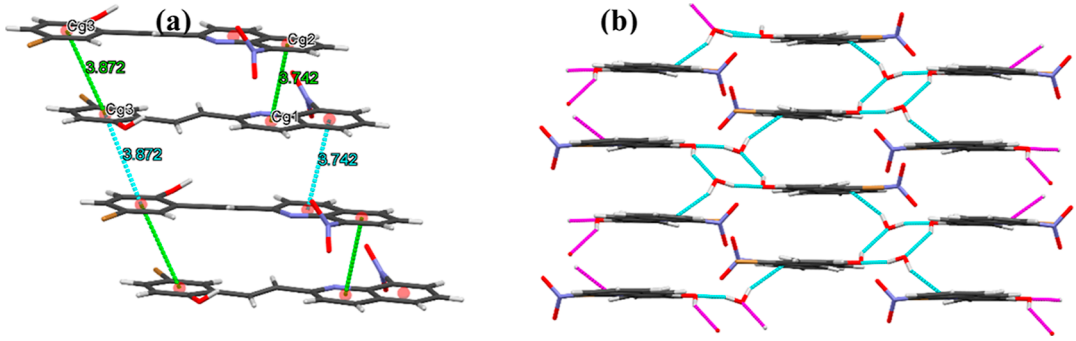

Figure 9. (a) π-Stacked dimers undergo further stacking interactions (turquoise dotted lines) in **S3B**, leading to chains; (b) the $\pi-\pi$ stacked chains are interconnected in a layered fashion through various H-bonding interactions (turquoise dotted lines). Hanging contacts are shown in pink.

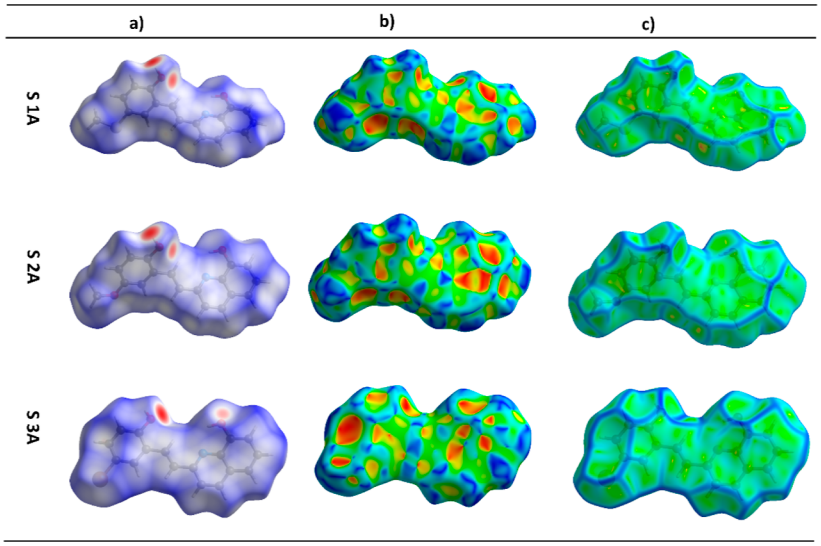

Figure 10. Hirshfeld surfaces mapped over (a) d_{norm}; (b) shape-index; and (c) curvedness of **S1A**−**S3A**.

N1···O4 interaction), as shown in Figure 8b. There are also $\pi-\pi$ stacking interactions between the adjacent molecules leading to chains, see Figure 9a. In these interactions, the centroid-to-centroid distances between the styryl rings are 3.872 Å, while the similar distances between the quinolyl rings are 3.742 Å. Unlike in **S1B** and **S2B**, these $\pi-\pi$ stacking interactions are not in a head-to-tail fashion. Another difference here is that the $\pi-\pi$ stacking interactions are not in a stepped fashion as observed in **S1B** and **S2B**. Intermolecular connections among the π-stacked chains through C2···O2 and N1···O4 interactions lead to a layered packing arrangement in the crystal lattice, see Figure 9b.

2.4. Hirshfeld Surface Analyses. Hirshfeld surface analyses were performed to get a qualitative and quantitative

https://doi.org/10.1021/acsomega.2c03047
ACS Omega 2022, 7, 24838−24850

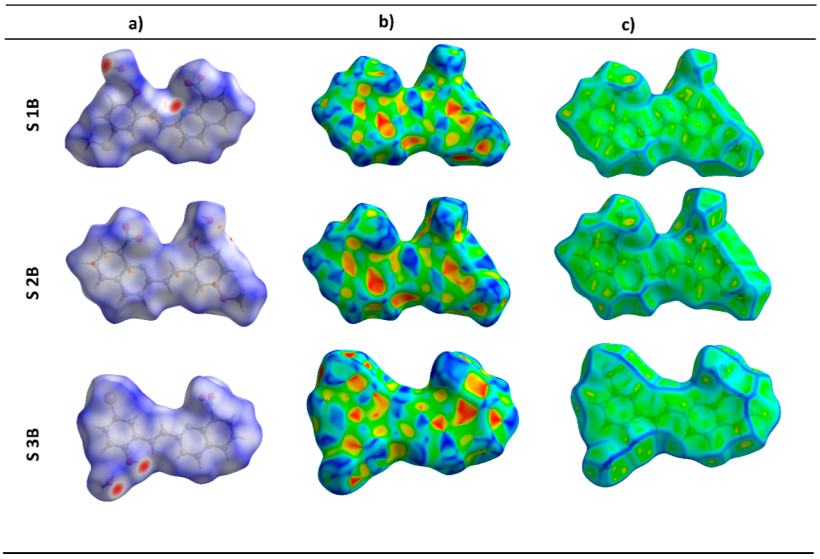

Figure 11. Hirshfeld surfaces mapped over (a) d_{norm}; (b) shape-index; and (c) curvedness of **S1B**−**S3B**.

understanding of the inter- and intra-molecular interactions in **SA** and **SB** series compounds.[57,58] A Hirshfeld surface can be mapped over d_{norm} ($d_{normalized}$), shape index, and curvedness, each providing different pieces of information about the interatomic interactions and crystal packing. The d_{norm} is a contact distance parameter that combines d_e (distance from the point to the nearest nucleus external to the surface), and d_i (distance to the nearest nucleus internal to the surface), and each is normalized by the van der Waals (vdW) radii of the atoms involved in the close contact. The Hirshfeld surface mapped over d_{norm} has different colors such as red, white, and blue. The red spot indicates interatomic interactions smaller than the sum of the vdW radii of the atoms involved in the contacts. In contrast, the white and blue spots correspond to the interatomic distances equal to or greater than the vdW radii of the atoms involved in the contacts.[59] The curvedness maps help to identify planar stacking interactions as relatively large green flat regions on such surfaces indicate the possibility of stacking interactions. The Hirshfeld surface mapped over the shape-index provides information regarding minute changes in the surface shape and highlights the regions where the two molecular Hirshfeld surfaces touch each other. The shape index maps use a red and blue color scheme for complementary pairs of hollows and bumps.

The Hirshfeld surfaces calculated for **S1A**−**S3A** and **S1B**−**S3B** are given in Figures 10 and 11. Different types of short-range interactions present in the crystal structure of these molecules can be seen on the Hirshfeld surface mapped over d_{norm} as red spots, see Figure 12. The most crucial feature here is the Hirshfeld surfaces that are simultaneously flat green on the curvedness maps and are patterned by red and blue triangles touching each other on the shape index maps, see Figures 10b and 11b. Such patterns indicate the presence of $\pi-\pi$ stacking between adjacent molecules. It can be noted that such patterns are visible in most of these molecules, suggesting the existence of $\pi-\pi$ stacking interactions as observed earlier by the crystal structure analyses.

The relative contributions of various intermolecular interactions to the Hirshfeld surface areas of **S1A**−**S3A** and **S1B**−**S3B** were calculated by analyzing the 2D fingerprint plots, as shown in Figures 13 and S41. These plots depict the

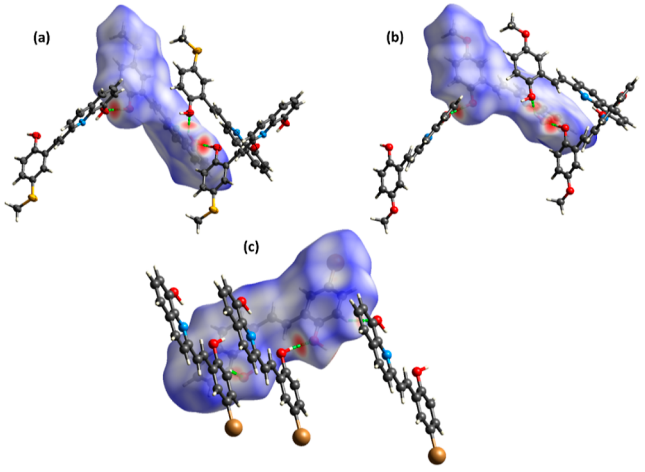

Figure 12. The short-range C−H···O interaction in (a) **S1A**; (b) **S2A**; and (c) **S3A**, respectively.

percentage contribution of each type of contact to the total Hirshfeld surface area. As shown, the significant contributions to the Hirshfeld surfaces come from H···H, C···H, and O···H interactions in all the cases with varying percentages. Another significant contribution is from C···C interactions. In the case of **SA** series compounds, the C···C interactions were in the range 6.8−8.8. However, in the case of **SB** series compounds, the relative contribution of C···C interactions was comparatively high, that is, 8.9−11.8. These interactions further highlight the existence of $\pi-\pi$ stacking interactions in these molecules and suggest that such interactions are more prominent in **SB** series compounds, probably due to their comparatively more planar molecular geometry.

2.5. Cytotoxicity Study. Studies on the cytotoxicity aspects of the **SA** and **SB** series compounds were conducted on human cervical carcinoma cell lines (HeLa cells) using the 3-(4,5-dimethylthiazol-2-yl)-2,5-diphenyl tetrazolium bromide (MTT) assay. 5×10^3 cells per well were plated and, after 24 h of incubation, treated with the dimethyl sulfoxide (DMSO) solubilized compounds **S1A**−**S3A**, and **S1B**−**S3B**, with a time frame of 48 h in a dose-dependent manner (0.5−50 μg/mL). The results summarized in Figures 14 and 15 and Table 1

https://doi.org/10.1021/acsomega.2c03047
ACS Omega 2022, 7, 24838−24850

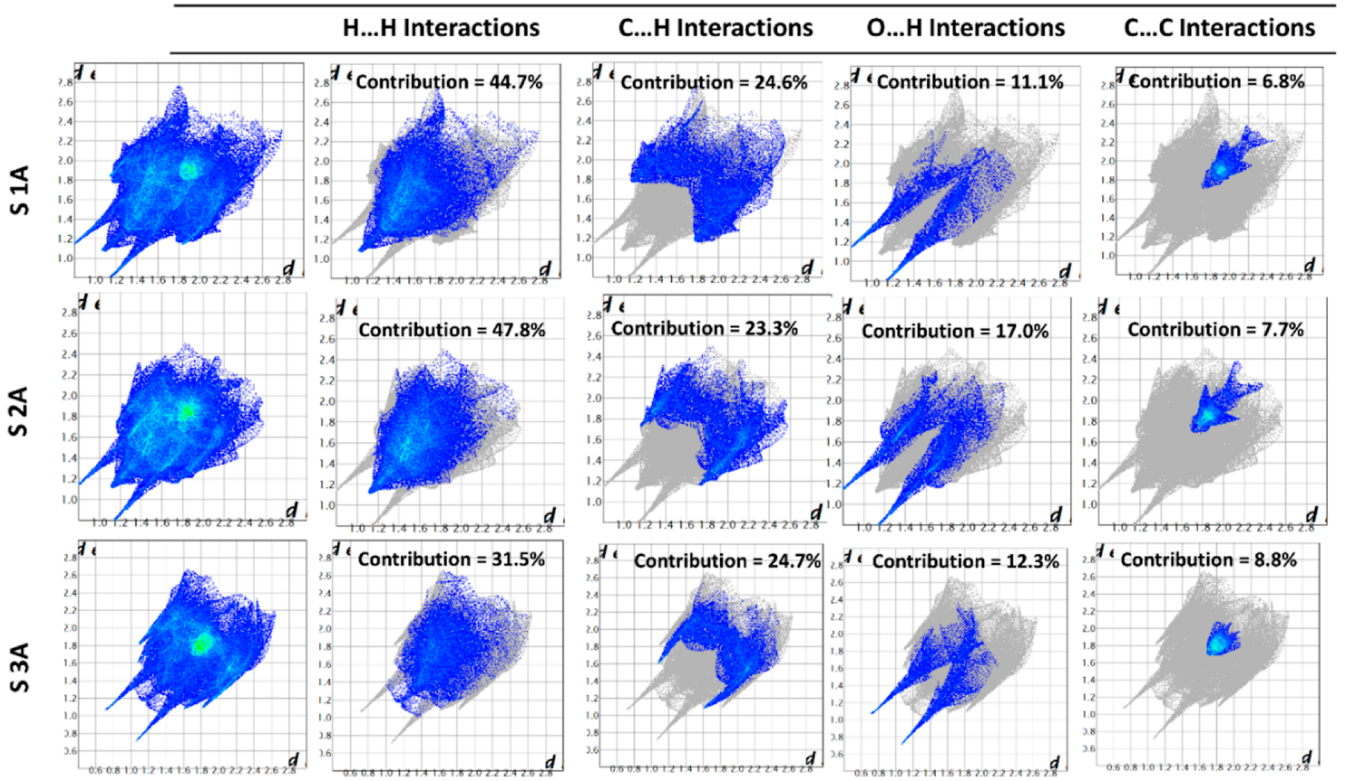

Figure 13. 2D fingerprint plot of **S1A**−**S3A** shows different types of interactions involved with their respective contribution.

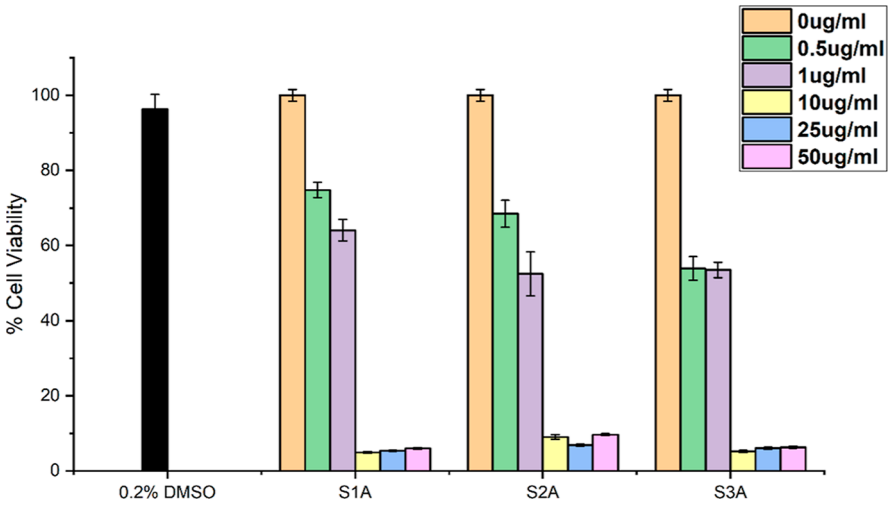

Figure 14. Cytotoxicity assay. **S1A**−**S3A** are incubated in HeLa cells for 48 h in a dosage-dependent manner.

show that most of the target compounds exhibited appreciable cytotoxicity against the HeLa cells.

The results of the cytotoxicity studies on the **SA** series compounds are presented in Figure 14. These compounds exhibited IC_{50} values in the 2.52−4.69 μM range against the tested cell line. The compound **S3A** exhibited a promising IC_{50} value of 2.52 μM in the series. The **SB** series compounds exhibited IC_{50} values in the range of 2.897−10.370 μM, indicating a comparatively lower cell inhibition property than the **SA** series compounds, see Figure 15. Compound **S3B** showed the best IC_{50} value of 2.897 μM in the series. Compared to **SB** series compounds, the **SA** series compounds exhibited better cytotoxicity with IC_{50} values of 2.52−4.69 μM. **S3A** was the most cytotoxic compound exhibiting the best IC_{50} value (2.52 μM) among the compounds tested in this study. The vehicle control DMSO (0.2%) showed no significant difference in cell cytotoxicity.

Analyses of the results show a pronounced effect of the substituents on the quinoline and the styryl rings in determining the cytotoxicity of these compounds. The **SA** series compounds having −OH substituent at the eighth position of the quinoline ring exhibited comparatively better performances than the **SB** series compounds with a $-NO_2$ substituent at the eighth position. Previous studies by Mrozek-Wilczkiewicz et al. on a panel of colon cancer cells (HCT 116) had also observed the importance of the hydroxyl group at the C8 position of quinoline. It was noted that the chelating properties due to the presence of the −OH group extend the

https://doi.org/10.1021/acsomega.2c03047
ACS Omega 2022, 7, 24838−24850

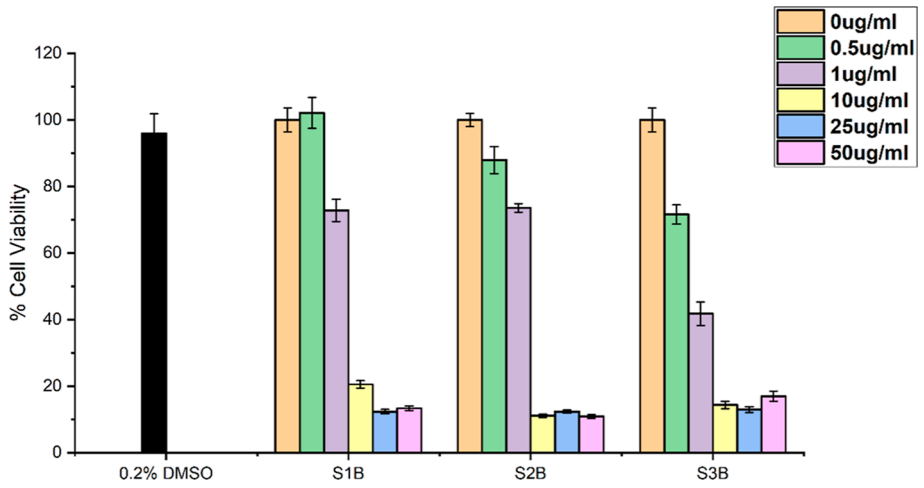

Figure 15. Cytotoxicity assay. **S1B**−**S3B** are incubated in HeLa cells for 48 h in a dosage-dependent manner.

Table 1. IC_{50} and IC_{90} Values of SA and SB Series Compounds against HeLa Cells

styryl derivate compound	IC_{50} (μM)	IC_{90} (μM)
S1A	4.694	30.066
S2A	3.859	44.342
S3A	2.518	36.694
S1B	10.370	75.439
S2B	7.653	52.975
S3B	2.897	83.222

activity of the styryl quinoline. While analyzing the effects of the substituents on the styryl ring, it is noted that the most active derivative (lowest IC_{50} value) in each series was the one bearing a −Br substituent. The derivatives bearing the $-OCH_3$ and $-SCH_3$ substituents on the styryl ring were less active in each series (see Table 1). This highlights the importance of an EWG halogen substituent on the styryl ring in determining the cytotoxicity of this class of compounds, as reported earlier.[14] Furthermore, it is evidenced that the introduction of additional EDGs (i.e., $-OCH_3$ and $-SCH_3$) on the styryl ring causes a reduction in the activity.

It can also be noted that the compounds studied here (**SA** and **SB** series) exhibited comparable or better cytotoxicity than many previously reported styryl quinoline derivatives (see Table S7 in the Supporting Information for a comparison). Compared to unsubstituted styryl quinoline derivatives, a series of styryl quinolines with halogenated styryl rings demonstrated improved activity and selectivity indices.[14] In the present study, we have not explored the detailed mechanistic aspects of cytotoxicity exhibited by **SA** and **SB** series compounds. However, we expect a mode of action as reported for similar styryl quinoline derivatives.[11,14] The significance of the hydroxyl group at the C-8 position for anticancer action also points to metal chelation as a possible mechanism reported for similar compounds.[14,60] However, more detailed mechanistic studies are required to establish the actual mode of action of the present compounds.

3. CONCLUSIONS

New series of 2S-8HQs and 2S-8NQs having different substituents on the styryl ring have been designed, synthesized, and structurally characterized. These new derivatives' structural, supramolecular, and cytotoxicity aspects have been studied and compared. The roles of various EDGs and EWGs on the styryl ring in deciding their properties have been analyzed. The cytotoxic assay on the HeLa cervical cancer cell line showed that the hydroxy analogues exhibit better cytotoxicity than the nitro analogues. These findings confirm the relevance of the hydroxyl group in position C-8 of quinoline. An EWG on the styryl ring of the molecule is required for high cytotoxicity levels. These new derivatives may therefore help understand the complex biological effects of styryl-quinolines. This study also attempted to establish styryl-quinolines as potential supramolecular synthons, especially for π-stacked structures, for the first time.

4. EXPERIMENTAL SECTION

4.1. Materials and Instrumentation. All the chemicals were purchased from Sigma-Aldrich. Solvents used were of spectroscopic grade and were used without further treatment. ^1H and ^{13}C NMR spectra were recorded on a Jeol-JNM 500 MHz NMR spectrometer using DMSO-d_6 and $CDCl_3$ as solvents and tetramethylsilane as the internal standard. High-resolution mass spectrometry (HR-MS) data were recorded on Bruker HD compact instrument.

4.2. Single Crystal X-ray Diffraction Analysis. Single-crystal X-ray data were collected on an Agilent SuperNova diffractometer, equipped with a multilayer optics monochromated dual source (Cu and Mo) and an Eos CCD detector, using Cu Kα radiation (1.54184 Å) at room temperature. Data acquisition, reduction, and absorption correction were performed by using CrysAlisPRO.[61] The structure was solved with ShelXS[62] program using direct methods and refined on F^2 by full-matrix least-squares techniques with ShelXL[62] through the Olex^2 (v.1.2) program package.[63] Anisotropic displacement parameters were applied for all the atoms, except for hydrogen atoms. The hydrogen atoms were placed in calculated positions and refined as riding atoms using isotropic displacement parameters. Due to the poor crystal quality, the crystal data of **S1A**, **S2A**, and **S2B** displayed some B level alerts in Checkcif. Specific explanations for the B-level alerts are given in the Supporting Information.

CCDC 2170717−2170722 contains the supplementary crystallographic data for this paper. These data can be obtained free of charge from The Cambridge Crystallographic Data Centre via www.ccdc.cam.ac.uk/data_request/cifdata.

https://doi.org/10.1021/acsomega.2c03047
ACS Omega 2022, 7, 24838−24850

Scheme 2. Overall Synthetic Scheme of Compounds S1A−S3A and S1B−S3B

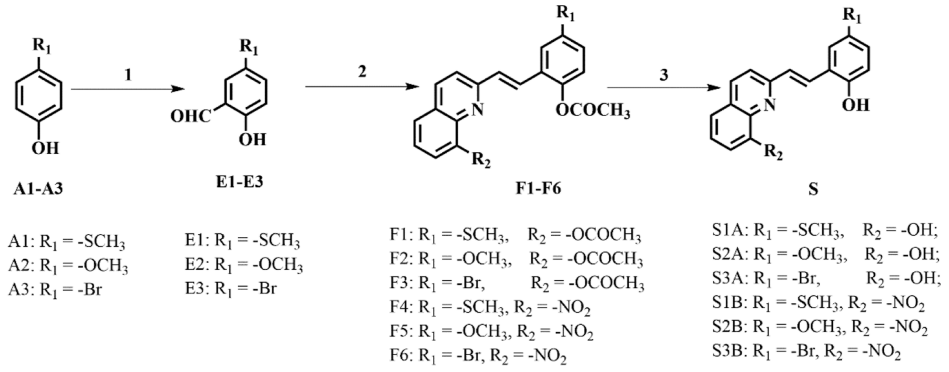

(1) Trifloroacetic acid, Hexamethylenetetramine, Reflux.
(2) 2-Methyl 8-OH/2-Methyl- 8-NO_2 quinoline, Acetic anhydride, Reflux.
(3) K_2CO_3, MeOH.

4.3. Hirshfeld Surface Analyses. To better understand and quantify the intra- and inter-molecular interactions present in the crystal structure of compounds, Hirshfeld surface analyses were performed using the Crystal explorer 17.5 program.[64] The Hirshfeld surfaces were drawn from the .cif files of the compounds, with a normalized contact distance (d_{norm}), which can be expressed as a combination of internal di, external de, and vdW radii of the atoms as below[47,48,65]

$$d_{norm} = \frac{(d_i - r_i^{vdW})}{r_i^{vdW}} + \frac{(d_e - r_e^{vdW})}{r_e^{vdW}}$$

4.4. Cell Viability Assay. The in vitro cytotoxicity of styryl derivatives was evaluated by MTT assay using HeLa cell line with a cell density of 5×10^4 cells per well. Cells were cultured in Dulbecco's modified Eagle medium (DMEM) containing 1% fetal bovine serum at 37 °C in 5% CO_2 in a 96 well plate. After cell adherence, media were replaced with new DMEM containing DMSO solubilized styryl derivatives in quadruples and incubated for 48 h. Cells without any treatment were selected as a positive control, with only media as negative control and 0.2% DMSO as vehicle control. 10% of MTT dye was added to evaluate the viability of cells. After incubation of 3 h, 100 μL of DMSO was added to each well and read at the absorbance of 570 nm with 650 nm as reference using Tecan Infinite M200 PRO plate reader.

*4.4.1. Synthesis of **SA** and **SB** Series Compounds.* As shown in Scheme 2, the target **SA** and **SB** series compounds were synthesized starting from 4-substituted phenol via a reported procedure.[49,50]

*4.4.2. General Procedure for the Synthesis of **E1**.* These compounds were synthesized by heating the 4-(methylthio) phenols (1 mmol) with hexamethylenetetramine (1.2 mmol) in trifluoroacetic acid at 130 °C for 24 h (TLC monitoring) following a reported procedure.[50] The products were purified by column chromatography using the ethyl acetate/hexane mixture.

E1 was obtained as a light-yellow solid in 45% yield. ^{1}H NMR (500 MHz, $CDCl_3$): δ ppm 10.82 (s, 1H), 9.77 (s, 1H), 7.40 (d, J = 4.85 Hz, 2H), 6.86 (d, J = 8.95 Hz, 1H), 2.39 (s, 3H). ^{13}C NMR (125 MHz): δ ppm 196.2, 160.0, 137.8, 133.4, 128.6, 121.0, 118.5, 17.9. MS (HR-MS) m/z: calcd for $C_8H_8O_2S$ ([M − H]), 167.02; found, 167.05.

*4.4.3. General Procedure for the Synthesis of **F1−F6**.* A mixture of compound **E** (1 mmol), 2-methyl-8-substituted quinoline (1 mmol), and acetic anhydride was heated at 130 °C under a nitrogen atmosphere for 24 h (TLC monitoring). After that, the reaction was quenched by pouring it into an ice-water mixture with stirring. The crude compound **F** thus separated was filtered, dried, and purified by recrystallization from ethyl acetate following a reported procedure.[49]

F1 was obtained as a brownish solid in 86% yield; ^{1}H NMR (500 MHz, $CDCl_3$): δ ppm 8.03 (d, J = 8.95 Hz, 2H), 7.55−7.62 (m, 2H), 7.48 (d, J = 8.95 Hz, 1H), 7.34−7.40 (m, 2H), 7.22 (d, J = 15.8 Hz, 1H), 7.14−7.17 (m, 1H), 6.97 (d, J = 8.95 Hz, 1H), 2.45 (s, 6H), 2.31 (s, 3H); ^{13}C NMR (125 MHz): δ ppm 169.8, 169.4, 155.3, 147.5, 146.6, 141.0, 136.6, 136.4, 131.6, 129.8, 128.8, 128.0, 127.7, 126.0, 125.7, 125.4, 123.4, 121.8, 120.6, 21.1, 21.0, 16.6. MS (HR-MS) m/z: calcd for $C_{22}H_{19}O_4NS$ ([M + H]$^+$), 394.10; found, 394.08.

F2 was obtained as a brown solid in 87% yield; ^{1}H NMR (500 MHz, $CDCl_3$): δ ppm 8.02 (d, J = 8.25 Hz, 1H), 7.62 (s, 1H), 7.57 (d, J = 9.65 Hz, 1H), 7.48 (d, J = 8.25 Hz, 1H), 7.33−7.39 (m, 2H), 7.21 (d, J = 15.8 Hz, 1H), 7.17 (d, J = 2.75 Hz, 1H), 6.95 (d, J = 8.95 Hz, 1H), 6.81 (dd, J = 8.95 Hz, 1H), 3.76 (s, 3H), 2.45 (s, 3H), 2.30 (s, 3H); ^{13}C NMR (125 MHz): δ ppm 169.8, 157.5, 155.5, 147.5, 142.6, 141.0, 136.5, 131.2, 130.0, 128.8, 128.1, 126.0, 125.7, 123.7, 121.7, 120.5, 115.5, 111.3, 55.8, 21.1, 20.0. MS (HR-MS) m/z: calcd for $C_{22}H_{19}O_5N$ ([M + H]$^+$), 378.12; found, 378.12.

F3 was obtained as a dark brown solid in 88% yield; ^{1}H NMR (500 MHz, $CDCl_3$): δ ppm 8.13 (d, J = 8.95 Hz, 1H), 7.86 (d, J = 2.75 Hz, 1H), 7.65−7.67 (m, 1H), 7.55 (dd, J = 7.9 Hz, 1H), 7.41−7.48 (m, 3H), 7.29 (s, 1H), 7.24−7.28 (m, 1H), 6.99 (dd, J = 8.25 Hz, 1H), 2.38 (s, 3H), 2.07 (s, 3H); ^{13}C NMR (125 MHz): δ ppm 170.0, 169.2, 155.0, 147.8, 147.6, 141.0, 136.8, 132.3, 132.2, 131.5, 130.0, 129.0, 126.8, 126.3, 125.7, 124.7, 122.0, 120.8, 119.7, 21.1, 20.7. MS (HR-MS) m/z: calcd for $C_{21}H_{16}O_4NBr$ ([M + H]$^+$), 426.02; found, 426.02.

F4 was obtained as a dark brown solid in 89% yield; ^{1}H NMR (500 MHz, $CDCl_3$): δ ppm 8.11 (dd, J = 8.25 Hz, 1H), 7.93 (dd, J = 13.05 Hz, 2H), 7.88 (d, J = 8.25 Hz, 2H), 7.58 (d, J = 2.05 Hz, 1H), 7.51 (dd, J = 8.2 Hz, 1H), 7.43−7.46 (m, 1H), 7.17−7.20 (m, 1H), 7.00 (dd, J = 8.25 Hz, 1H), 2.46 (s, 3H), 2.41 (s, 3H); ^{13}C NMR (125 MHz): δ ppm 169.9, 157.2, 148.2, 147.0, 139.6, 136.6, 136.5, 131.7, 129.5, 129.2, 129.1,

https://doi.org/10.1021/acsomega.2c03047
ACS Omega 2022, 7, 24838−24850

128.5, 128.3, 124.9, 124.7, 124.1, 123.6, 122.4, 21.0, 16.6. MS (HR-MS) m/z: calcd for $C_{20}H_{16}O_4N_2S$ ($[M + H]^+$), 381.08; found, 381.09.

F5 was obtained as a brown solid in 90% yield; ^{1}H NMR (500 MHz, $CDCl_3$): δ ppm 8.11 (d, J = 8.95 Hz, 1H), 7.88−7.94 (m, 3H), 7.53 (d, J = 8.25 Hz, 1H), 7.43−7.46 (m, 1H), 7.20 (dd, J = 15.8 Hz, 2H), 6.98 (d, J = 8.95 Hz, 1H), 6.83−6.86 (m, 1H), 3.79 (s, 3H), 2.39 (s, 3H); ^{13}C NMR (125 MHz): δ ppm 170.2, 157.6, 157.4, 148.2, 143.1, 139.7, 136.6, 131.6, 130.1, 129.4, 129.0, 128.13, 124.7, 124.1, 123.9, 122.3, 116.2, 110.9, 55.9, 21.0. MS (HR-MS) m/z: calcd for $C_{20}H_{16}O_5N_2$ ($[M + H]^+$), 365.11; found, 365.11.

F6 was obtained as a brown solid in 87% yield; ^{1}H NMR (500 MHz, $CDCl_3$): δ ppm 8.12 (d, J = 8.25 Hz, 1H), 7.96 (d, J = 7.6 Hz, 1H), 782−7.89 (m, 2H), 7.41−7.50 (m, 4H), 7.13 (dd, J = 16.5 Hz, 1H), 7.00 (d, J = 8.95 Hz, 1H), 2.48 (s, 3H); ^{13}C NMR (125 MHz): δ ppm 169.5, 156.6, 148.1, 148.0, 139.4, 136.7, 132.6, 131.7, 130.7, 129.4, 129.3, 128.3, 124.8, 124.7, 124.0, 122.6, 119.46, 117.6, 20.9. MS (HR-MS) m/z: calcd for $C_{19}H_{13}O_4N_2Br$ ($[(M + 2) + H]^+$), 415.00; found, 414.99.

*4.4.4. General Procedure for the Synthesis of **S1A**−**S3A** and **S1B**−**S3B**.* To a solution of the corresponding compound **F** (1 mmol) in methanol was added K_2CO_3 (1.5 mmol), and the reaction mixture was stirred at room temperature for 120 min. After completing the reaction, as monitored by TLC, the reaction mixture was poured into water and neutralized with HCl solution, and the precipitate was filtered and dried. The crude product thus obtained was purified by recrystallization from ethanol.

S1A was obtained as a brown solid in 87% yield. ^{1}H NMR (500 MHz, DMSO-d_6): δ ppm 10.14 (s, 1H), 9.57 (s, 1H), 8.26 (d, J = 8.95 Hz, 1H), 8.09 (d, J = 16.45 Hz, 1H), 7.78 (d, J = 8.95 Hz, 1H), 7.59 (d, J = 2.75 Hz, 1H), 7.56 (s, 1H), 7.33−7.38 (m, 2H), 7.27 (d, J = 2.05 Hz, 1H), 7.09 (d, J = 16.45 Hz, 1H), 6.94 (d, J = 8.95 Hz, 1H), 2.50 (s, 3H); ^{13}C NMR (125 MHz): δ ppm 154.6, 154.1, 153.0, 138.3, 136.4, 129.8, 129.7, 129.0, 127.9, 127.7, 126.9, 126.8, 124.0, 120.6, 117.6, 117.0, 111.3, 17.0. HRMS m/z: calcd for $C_{18}H_{15}O_2NS$ $[M + H]^+$, 310.08; found, 310.07.

S2A was obtained as a light yellow solid in 85% yield. ^{1}H NMR (500 MHz, DMSO-d_6): δ ppm 9.55 (s, 1H), 8.26 (d, J = 8.95 Hz, 1H), 8.08 (d, J = 16.45 Hz, 1H), 7.78 (d, J = 8.9 Hz, 1H), 7.53 (d, J = 15.8 Hz, 1H), 7.34−7.39 (m, 2H), 7.20 (d, J = 3.45 Hz, 1H), 7.08 (dd, J = 8.9 Hz, 1H), 6.86 (d, J = 8.95 Hz, 1H), 6.78−6.80 (m, 1H), 3.75 (s, 3H); ^{13}C NMR (125 MHz): δ ppm 154.2, 152.9, 152.3, 150.0, 138.2, 136.4, 130.0, 128.4, 127.6, 126.8, 123.4, 120.3, 117.6, 116.9, 116.1, 111.6, 116.3, 55.4. HRMS m/z: calcd for $C_{18}H_{15}O_3N$ $[M - H]$, 292.10; found, 292.10.

S3A was obtained as a dark brown solid in 87% yield. ^{1}H NMR (500 MHz, DMSO-d_6): δ ppm 8.24 (d, J = 8.90 Hz, 1H), 8.08 (d, J = 16.5 Hz, 1H), 7.75 (d, J = 8.95 Hz, 1H), 7.72 (d, J = 2.75 Hz, 1H), 7.62 (d, J = 16.5 Hz, 1H), 7.32−7.38 (m, 2H), 7.24 (d, J = 8.9 Hz, 1H), 7.08 (d, J = 6.85 Hz, 1H), 6.91 (d, J = 8.25 Hz, 1H); ^{13}C NMR (125 MHz): δ ppm 157.7, 154.2, 153.0, 138.3, 136.4, 131.7, 130.4, 129.8, 128.8, 127.6, 126.8, 125.7, 120.6, 118.8, 117.5, 111.3, 108.8. HRMS m/z: calcd for $C_{17}H_{12}O_2NBr$ $[M + H]^+$, 342.00; found, 342.04.

S1B was obtained as a dark brown solid in 88% yield. ^{1}H NMR (500 MHz, DMSO-d_6): δ ppm 10.19 (s, 1H), 8.52 (d, J = 8.95 Hz, 1H), 8.22−8.24 (m, 2H), 8.04 (s, 1H), 7.97−8.00 (m, 1H), 7.64−7.69 (m, 2H), 7.52 (d, J = 16.5 Hz, 1H), 7.18 (d, J = 8.25 Hz, 1H), 6.92 (d, J = 8.25 Hz, 1H), 2.50 (s, 3H); ^{13}C NMR (125 MHz): δ ppm 158.1, 154.6, 147.6, 138.5, 137.0, 131.7, 130.3, 127.8, 127.6, 127.23, 127.0, 125.0, 123.5, 123.4, 122.0, 116.9, 16.8. HRMS m/z: calcd for $C_{18}H_{14}O_3N_2S$ $[M - H]$, 337.07; found, 337.10.

S2B was obtained as a dark brown solid in 87% yield. ^{1}H NMR (500 MHz, DMSO-d_6): δ ppm 9.66 (s, 1H), 8.51 (d, J = 8.95 Hz, 1H), 8.22 (dd, J = 8.25 Hz, 2H), 8.05 (d, J = 16.5 Hz, 1H), 7.98 (d, J = 8.95 Hz, 1H), 7.67 (t, J = 7.9 Hz, 1H), 7.47 (d, J = 16.45 Hz, 1H), 7.25 (d, J = 2.72 Hz, 1H), 6.81−6.88 (m, 2H), 3.76 (s, 3H); ^{13}C NMR (125 MHz): δ ppm 158.2, 152.3, 150.2, 147.6, 138.5, 136.9, 131.8, 131.7, 127.6, 127.2, 124.9, 123.5, 122.8, 121.8, 117.2, 111.0, 55.5. HRMS m/z: calcd for $C_{18}H_{14}O_4N_2$ $[M + H]^+$, 323.10; found, 323.12.

S3B was obtained as a reddish solid in 88% yield. ^{1}H NMR (500 MHz, DMSO-d_6): δ ppm 10.60 (s, 1H), 8.52 (d, J = 8.25 Hz, 1H), 8.22 (d, J = 7.55 Hz, 2H), 7.95−7.8.00 (m, 2H), 7.86 (s, 1H), 7.65−7.68 (m, 1H), 7.53 (d, J = 15.8 Hz, 1H), 7.33 (d, J = 7.55 Hz, 1H), 6.94 (d, J = 7.55 Hz, 1H). ^{13}C NMR (125 MHz): δ ppm 157.8, 155.5, 147.6, 138.4, 137.0, 132.5, 131.7, 130.3, 129.8, 128.4, 127.7, 125.1, 125.0, 123.6, 122.1, 118.3, 110.7. HRMS m/z: calcd for $C_{17}H_{11}O_3N_2Br$ $[M + H]^+$, 371.00; found, 371.03.

■ ASSOCIATED CONTENT

Supporting Information

The Supporting Information is available free of charge at https://pubs.acs.org/doi/10.1021/acsomega.2c03047.

NMR spectra, HR-MS, crystallographic data, and additional crystallographic information (PDF)

Crystallographic data of **S1A** (CIF)

Crystallographic data of **S1B** (CIF)

Crystallographic data of **S2A** (CIF)

Crystallographic data of **S2B** (CIF)

Crystallographic data of **S3A** (CIF)

Crystallographic data of **S3B** (CIF)

■ AUTHOR INFORMATION

Corresponding Authors

Neha Garg − *Department of Medicinal Chemistry, Faculty of Ayurveda, Institute of Medical Sciences, Banaras Hindu University, Varanasi 221005 Uttar Pradesh, India;* orcid.org/0000-0003-2227-8292; Email: nehagarg@bhu.ac.in

Chullikkattil P. Pradeep − *School of Basic Sciences, Indian Institute of Technology Mandi, Kamand 175005 Himachal Pradesh, India;* orcid.org/0000-0002-5811-8509; Phone: +91 1905 267 045; Email: pradeep@iitmandi.ac.in; Fax: +91 1905 267 009

Authors

Suman Sehlangia − *School of Basic Sciences, Indian Institute of Technology Mandi, Kamand 175005 Himachal Pradesh, India*

Namyashree Nayak − *School of Basic Sciences, Indian Institute of Technology Mandi, Kamand 175005 Himachal Pradesh, India*

Complete contact information is available at: https://pubs.acs.org/10.1021/acsomega.2c03047

Author Contributions

S.S. synthesized and characterized the compounds and wrote the draft of the paper under the supervision of C.P.P. The cytotoxic studies were performed by N.N. under the supervision of N.S. The overall project was conceived and the manuscript finalized by C.P.P.

Notes

The authors declare no competing financial interest.

■ ACKNOWLEDGMENTS

C.P.P. thanks SERB, Govt. of India, for financial support (project no. EMR/2016/002334) and AMRC, IIT Mandi for infrastructural facilities. S.S. thanks MHRD, Government of India, for a fellowship. N.N. acknowledges a fellowship from SERB (ECR/2017/000926). N.G. acknowledges SERB grant (ECR/2017/000926) and seed grant under IOE, Banaras Hindu University.

■ REFERENCES

(1) Gupta, R.; Luxami, V.; Paul, K. Insights of 8-hydroxyquinolines: A novel target in medicinal chemistry. *Bioorg. Chem.* **2021**, *108*, 104633.

(2) Song, Y. n.; Xu, H.; Chen, W.; Zhan, P.; Liu, X. 8-Hydroxyquinoline: a privileged structure with a broad-ranging pharmacological potential. *MedChemComm* **2015**, *6*, 61−74.

(3) Huo, Y.; Lu, J.; Hu, S.; Zhang, L.; Zhao, F.; Huang, H.; Huang, B.; Zhang, L. Photoluminescence properties of new Zn(II) complexes with 8-hydroxyquinoline ligands: Dependence on volume and electronic effect of substituents. *J. Mol. Struct.* **2015**, *1083*, 144−151.

(4) Skotheim, T. A.; Reynold, J. *Handbook of Conducting Polymers*, 3rd ed.; CRC Press: New York, 2007.

(5) Gao, W.; Li, Z.; Xu, Q.; Li, Y. First synthesis of novel 2,4-bis((E)-styryl)quinoline-3-carboxylate derivatives and their antitumor activity. *RSC Adv.* **2018**, *8*, 38844−38849.

(6) El-Sayed, M. A.-A.; El-Husseiny, W. M.; Abdel-Aziz, N. I.; El-Azab, A. S.; Abuelizz, H. A.; Abdel-Aziz, A. A.-M. Synthesis and biological evaluation of 2-styrylquinolines as antitumour agents and EGFR kinase inhibitors: molecular docking study. *J. Enzyme Inhib. Med. Chem.* **2018**, *33*, 199−209.

(7) Luczywo, A.; Sauter, I. P.; da Silva Ferreira, T. C.; Cortez, M.; Romanelli, G. P.; Sathicq, G.; Asís, S. E. Microwave-assisted synthesis of 2-styrylquinoline-4-carboxylic acid derivatives to improve the toxic effect against Leishmania (Leishmania) amazonensis. *J. Heterocycl. Chem.* **2021**, *58*, 822−832.

(8) Staderini, M.; Piquero, M.; Abengózar, M. Á.; Nachér-Vázquez, M.; Romanelli, G.; López-Alvarado, P.; Rivas, L.; Bolognesi, M. L.; Menéndez, J. C. Structure-activity relationships and mechanistic studies of novel mitochondria-targeted, leishmanicidal derivatives of the 4-aminostyrylquinoline scaffold. *Eur. J. Med. Chem.* **2019**, *171*, 38−53.

(9) Musiol, R. Styrylquinoline—A Versatile Scaffold in Medicinal Chemistry. *Med. Chem.* **2020**, *16*, 141−154.

(10) Sehlangia, S.; Sharma, S.; Sharma, S. K.; Pradeep, C. P. 2,2′-(Arylenedivinylene)bis-8-hydroxyquinolines exhibiting aromatic $\pi-\pi$ stacking interactions as solution-processable p-type organic semiconductors for high-performance organic field effect transistors. *Mater. Adv.* **2021**, *2*, 4643−4651.

(11) Mrozek-Wilczkiewicz, A.; Kuczak, M.; Malarz, K.; Cieślik, W.; Spaczyńska, E.; Musiol, R. The synthesis and anticancer activity of 2-styrylquinoline derivatives. A p53 independent mechanism of action. *Eur. J. Med. Chem.* **2019**, *177*, 338−349.

(12) Podeszwa, B.; Niedbala, H.; Polanski, J.; Musiol, R.; Tabak, D.; Finster, J.; Serafin, K.; Milczarek, M.; Wietrzyk, J.; Boryczka, S.; Mol, W.; Jampilek, J.; Dohnal, J.; Kalinowski, D. S.; Richardson, D. R. Investigating the antiproliferative activity of quinoline-5,8-diones and styrylquinolinecarboxylic acids on tumor cell lines. *Bioorg. Med. Chem. Lett.* **2007**, *17*, 6138−6141.

(13) Chang, F.-S.; Chen, W.; Wang, C.; Tzeng, C.-C.; Chen, Y.-L. Synthesis and antiproliferative evaluations of certain 2-phenylvinylquinoline (2-styrylquinoline) and 2-furanylvinylquinoline derivatives. *Bioorg. Med. Chem.* **2010**, *18*, 124−133.

(14) Mrozek-Wilczkiewicz, A.; Spaczynska, E.; Malarz, K.; Cieslik, W.; Rams-Baron, M.; Kryštof, V.; Musiol, R. Design, Synthesis and In Vitro Activity of Anticancer Styrylquinolines. The p53 Independent Mechanism of Action. *PLoS One* **2015**, *10*, No. e0142678.

(15) Ouali, M.; Laboulais, C.; Leh, H.; Gill, D.; Desmaële, D.; Mekouar, K.; Zouhiri, F.; d'Angelo, J.; Auclair, C.; Mouscadet, J.-F.; Le Bret, M. Modeling of the Inhibition of Retroviral Integrases by Styrylquinoline Derivatives. *J. Med. Chem.* **2000**, *43*, 1949−1957.

(16) Polanski, J.; Zouhiri, F.; Jeanson, L.; Desmaële, D.; d'Angelo, J.; Mouscadet, J.-F.; Gieleciak, R.; Gasteiger, J.; Le Bret, M. Use of the Kohonen Neural Network for Rapid Screening of Ex Vivo Anti-HIV Activity of Styrylquinolines. *J. Med. Chem.* **2002**, *45*, 4647−4654.

(17) Cieslik, W.; Musiol, R.; Nycz, J. E.; Jampilek, J.; Vejsova, M.; Wolff, M.; Machura, B.; Polanski, J. Contribution to investigation of antimicrobial activity of styrylquinolines. *Bioorg. Med. Chem.* **2012**, *20*, 6960−6968.

(18) Szczepaniak, J.; Cieślik, W.; Romanowicz, A.; Musioł, R.; Krasowska, A. Blocking and dislocation of Candida albicans Cdr1p transporter by styrylquinolines. *Int. J. Antimicrob. Agents* **2017**, *50*, 171−176.

(19) Roberts, B. F.; Zheng, Y.; Cleaveland, J.; Lee, S.; Lee, E.; Ayong, L.; Yuan, Y.; Chakrabarti, D. 4-Nitro styrylquinoline is an antimalarial inhibiting multiple stages of Plasmodium falciparum asexual life cycle. *Int. J. Parasitol.: Drugs Drug Resist.* **2017**, *7*, 120−129.

(20) Wang, X.-Q.; Xia, C.-L.; Chen, S.-B.; Tan, J.-H.; Ou, T.-M.; Huang, S.-L.; Li, D.; Gu, L.-Q.; Huang, Z.-S. Design, synthesis, and biological evaluation of 2-arylethenylquinoline derivatives as multifunctional agents for the treatment of Alzheimer's disease. *Eur. J. Med. Chem.* **2015**, *89*, 349−361.

(21) Staderini, M.; Aulić, S.; Bartolini, M.; Ngoc, H.; Tran, A.; Gonzaíez-Ruiz, V.; Perez, D. I.; Cabezas, N.; Martínez, A.; Martin, M. A.; Andrisano, V.; Legname, G.; Menéndez, J. C.; Bolognesi, M. L. A Fluorescent Styrylquinoline with Combined Therapeutic and Diagnostic Activities against Alzheimer's and Prion Diseases. *ACS Med. Chem. Lett.* **2013**, *4*, 225−229.

(22) Wang, T.-T.; Zeng, G.-C.; Zeng, H.-P.; Liu, P.-Y.; Wang, R.-X.; Zhang, Z.-J.; Xiong, Y.-L. Synthesis of light-emmting materials bis-[2′-2″-(9H-fluoren-2-yl)-vinyl-8-hydroxyquinoline] zinc(II) and bis-[2′-4″-(4,5-diphenyl-1H-imidazol-2-yl)styryl-8-hydroxyquinoline] zinc-(II). *Tetrahedron* **2009**, *65*, 6325−6329.

(23) Zeng, H.-P.; Wang, G.-R.; Zeng, G.-C.; Li, J. The synthesis, characterization and electroluminescent properties of zinc(II) complexes for single-layer organic light-emitting diodes. *Dyes Pigm.* **2009**, *83*, 155−161.

(24) Zeng, H.-P.; OuYang, X.-H.; Wang, T.-T.; Yuan, G.-Z.; Zhang, G.-H.; Zhang, X.-m. Synthesis, Crystal Structure, and Prediction of Hole Mobilities of 2,7′-Ethylenebis(8-hydroxyquinoline). *Cryst. Growth Des.* **2006**, *6*, 1697−1702.

(25) Gavrishova, T. N.; Budyka, M. F. Synthesis of symmetric and asymmetric bichromophoric styrylbenzo[f]quinoline dyads with a 1,2-phenylene and 2,3-naphthylene framework. *Russ. Chem. Bull.* **2019**, *68*, 583−587.

(26) Huo, Y.; Lu, J.; Lu, T.; Fang, X.; Ouyang, X.; Zhang, L.; Yuan, G. Comparative studies on OLED performances of chloro and fluoro substituted Zn(II) 8-hydroxyquinolinates. *New J. Chem.* **2015**, *39*, 333−341.

(27) Barberis, V. P.; Mikroyannidis, J. A. Synthesis and optical properties of aluminum and zinc quinolates through styryl subsituent in 2-position. *Synth. Met.* **2006**, *156*, 865−871.

(28) Ouyang, X.; Wang, G.; Zeng, H.; Zhang, W.; Li, J. Design and synthesis of 2-substituted-8-hydroxyquinline zinc complexes with hole-transporting ability for highly effective yellow-light emitters. *J. Organomet. Chem.* **2009**, *694*, 3511−3517.

https://doi.org/10.1021/acsomega.2c03047
ACS Omega 2022, 7, 24838−24850

(29) Zhou, Y.; Jie, K.; Zhao, R.; Huang, F. Supramolecular-Macrocycle-Based Crystalline Organic Materials. *Adv. Mater.* **2020**, *32*, 1904824.
(30) Seidi, F.; Shamsabadi, A. A.; Amini, M.; Shabanian, M.; Crespy, D. Functional materials generated by allying cyclodextrin-based supramolecular chemistry with living polymerization. *Polym. Chem.* **2019**, *10*, 3674−3711.
(31) Webber, M. J.; Langer, R. Drug delivery by supramolecular design. *Chem. Soc. Rev.* **2017**, *46*, 6600−6620.
(32) Zhao, L.; Liu, Y.; Xing, R.; Yan, X. Supramolecular Photothermal Effects: A Promising Mechanism for Efficient Thermal Conversion. *Angew. Chem., Int. Ed.* **2020**, *59*, 3793−3801.
(33) Liang, F.; Chen, J.; Cheng, Y.; Wang, L.; Ma, D.; Jing, X.; Wang, F. Synthesis, characterization, photoluminescent and electroluminescent properties of new conjugated 2,2′-(arylenedivinylene)bis-8-substituted quinolines. *J. Mater. Chem.* **2003**, *13*, 1392−1399.
(34) Zhang, X.; Li, S.; Zhang, Z.; Liao, C.; Li, Q. Synthesis of 8-Hydroxyquinoline Derivative and Its Zinc Complex. *J. Comput. Theor. Nanosci.* **2015**, *12*, 2786−2790.
(35) Huo, Y.; Pan, C.; Wang, S.; Ji, S.; Kong, T.; Gao, L.; Cai, N.; Zeng, H. Color-tunable solid-state emissions of Zn(II) and Cd(II) complexes derived from cyano-modified 2-substituted 8-hydroxyquinolines. *Polyhedron* **2016**, *119*, 175−183.
(36) Huo, Y.; Wang, C.; Lu, J.; Hu, S.; Li, X.; Zhang, L. A novel trimeric Zn (II) complex based on 8-hydroxyquinoline with trifluoromethylbenzene group: Synthesis, crystal structure, photophysical properties and DNA binding. *J. Mol. Struct.* **2015**, *1098*, 311−317.
(37) Pan, C.; Yang, B.; Wang, F.; Xu, J.; Chen, G.; Ji, W.; Huo, Y. Anion-tuned assembly of three double cubane tetranuclear Cd(II)/Zn(II) complexes based on a 2-substituted 8-hydroxyquinoline ligand: Synthesis, crystal structures and fluorescent properties. *J. Mol. Struct.* **2020**, *1212*, 127770.
(38) Gong, C.; Zhang, J.; Zeng, X.; Xie, J. Highly effective synthesis of a cobalt(ii) metal-organic coordination polymer by using continuous flow chemistry. *Dalton Trans.* **2017**, *46*, 25−28.
(39) Zhang, J.; Xie, Y. R.; Ye, Q.; Xiong, R. G.; Xue, Z.; You, X. Z. Blue to Red Fluorescent Emission Tuning of a Cadmium Coordination Polymer by Conjugated Ligands. *Eur. J. Inorg. Chem.* **2003**, *2003*, 2572−2577.
(40) Zhao, X.; Wang, S.; Zhang, L.; Liu, S.; Yuan, G. 8-Hydroxyquinolinate-Based Metal-Organic Frameworks: Synthesis, Tunable Luminescent Properties, and Highly Sensitive Detection of Small Molecules and Metal Ions. *Inorg. Chem.* **2019**, *58*, 2444−2453.
(41) Yuan, G.; Huo, Y.; Nie, X.; Jiang, H.; Liu, B.; Fang, X.; Zhao, F. Controllable supramolecular structures and luminescent properties of unique trimeric Zn(II) 8-hydroxyquinolinates tuned by functional substituents. *Dalton Trans.* **2013**, *42*, 2921−2929.
(42) Yuan, G.; Zhang, Q.; Wang, Z.; Song, K.; Yuan, X.; Wang, Y.; Zhang, L. Assembly of four 8-quinolinate-based multinuclear complexes: the effect of substituents on core structures and photoluminescence properties. *Inorg. Chem. Front.* **2017**, *4*, 764−772.
(43) Bell, J.; Samb, I.; Toullec, P. Y.; Mongin, O.; Blanchard-Desce, M.; Michelet, V.; Leray, I. Ultra-sensitive and selective Hg^{2+} chemosensors derived from substituted 8-hydroxyquinoline analogues. *New J. Chem.* **2014**, *38*, 1072−1078.
(44) Yuan, G.-Z.; Huo, Y.-P.; Nie, X.-L.; Fang, X.-M.; Zhu, S.-Z. Structure and photophysical properties of a dimeric Zn(II) complex based on 8-hydroxyquinoline group containing 2,6-dichlorobenzene unit. *Tetrahedron* **2012**, *68*, 8018−8023.
(45) Machura, B.; Wolff, M.; Kowalczyk, W.; Musiol, R. Novel rhenium(V) complexes of 8-hydroxyquinoline derivatives - Synthesis, spectroscopic characterization, X-ray structure and DFT calculations. *Polyhedron* **2012**, *33*, 388−395.
(46) Fang, X.-M.; Huo, Y.-P.; Wei, Z.-G.; Yuan, G.-Z.; Huang, B.-H.; Zhu, S.-Z. Impact of substituents on the luminescent properties and thermostability of Zn(II) 8-hydroxyquinolinates: insight from experimental and theoretical approach. *Tetrahedron* **2013**, *69*, 10052−10059.
(47) McKinnon, J. J.; Spackman, M. A.; Mitchell, A. S. Novel tools for visualizing and exploring intermolecular interactions in molecular crystals. *Acta Crystallogr., Sect. B: Struct. Sci.* **2004**, *60*, 627−668.
(48) Sosorev, A. Y.; Trukhanov, V. A.; Maslennikov, D. R.; Borshchev, O. V.; Polyakov, R. A.; Skorotetcky, M. S.; Surin, N. M.; Kazantsev, M. S.; Dominskiy, D. I.; Tafeenko, V. A.; Ponomarenko, S. A.; Paraschuk, D. Y. Fluorinated Thiophene-Phenylene Co-Oligomers for Optoelectronic Devices. *ACS Appl. Mater. Interfaces* **2020**, *12*, 9507−9519.
(49) Sharghi, H.; Nasseri, M. A.; Niknam, K. Phenol-Containing Macrocyclic Diamides as New Catalysts in the Highly Regioselective Conversion of Epoxides to β-Hydroxy Thiocyanates. *J. Org. Chem.* **2001**, *66*, 7287−7293.
(50) Sehlangia, S.; Devi, M.; Nayak, N.; Garg, N.; Dhir, A.; Pradeep, C. P. Synthesis, Crystal Structure and Substituent Controlled Photoluminescence and Chemosensing Properties of a Series of 2,2′-(Arylenedivinylene)bis-8-hydroxyquinolines. *ChemistrySelect* **2020**, *5*, 5429−5436.
(51) Xu, F.; Khan, I. J.; McGuinness, K.; Parmar, A. S.; Silva, T.; Murthy, N. S.; Nanda, V. Self-Assembly of Left- and Right-Handed Molecular Screws. *J. Am. Chem. Soc.* **2013**, *135*, 18762−18765.
(52) Zhou, Z.; Giles, K. E.; Felsenfeld, G. DNA·RNA triple helix formation can function as a cis -acting regulatory mechanism at the human β-globin locus. *Proc. Natl. Acad. Sci. U.S.A.* **2019**, *116*, 6130−6139.
(53) Barrie, J.; Zawdie, G.; João, E. Assessing the role of triple helix system intermediaries in nurturing an industrial biotechnology innovation network. *J. Cleaner Prod.* **2019**, *214*, 209−223.
(54) Brown, J. A. Unraveling the structure and biological functions of RNA triple helices. *Wiley Interdiscip. Rev.: RNA* **2020**, *11*, No. e1598.
(55) Conrad, N. K. The emerging role of triple helices in RNA biology. *Wiley Interdiscip. Rev.: RNA* **2014**, *5*, 15−29.
(56) Stephenson, A.; Ward, M. D. A triple helix of double helicates: three hierarchical levels of self-assembly in a single structure. *Chem. Commun.* **2012**, *48*, 3605−3607.
(57) McKinnon, J. J.; Spackman, M. A.; Mitchell, A. S. Novel tools for visualizing and exploring intermolecular interactions in molecular crystals. *Acta Crystallogr., Sect. B: Struct. Sci.* **2004**, *60*, 627−668.
(58) Spackman, M. A.; Byrom, P. G. A novel definition of a molecule in a crystal. *Chem. Phys. Lett.* **1997**, *267*, 215−220.
(59) Sosorev, A. Y.; Trukhanov, V. A.; Maslennikov, D. R.; Borshchev, O. V.; Polyakov, R. A.; Skorotetcky, M. S.; Surin, N. M.; Kazantsev, M. S.; Dominskiy, D. I.; Tafeenko, V. A.; Ponomarenko, S. A.; Paraschuk, D. Y. Fluorinated Thiophene-Phenylene Co-Oligomers for Optoelectronic Devices. *ACS Appl. Mater. Interfaces* **2020**, *12*, 9507−9519.
(60) Barilli, A.; Atzeri, C.; Bassanetti, I.; Ingoglia, F.; Dall'Asta, V.; Bussolati, O.; Maffini, M.; Mucchino, C.; Marchiò, L. Oxidative stress induced by copper and iron complexes with 8-hydroxyquinoline derivatives causes paraptotic death of HeLa cancer cells. *Mol. Pharm.* **2014**, *11*, 1151−1163.
(61) *CrysAlisPro Program*, version 171.37.33c; Agilent Technologies: Oxford, UK, 2012.
(62) Sheldrick, G. M. A short history of SHELX. *Acta Crystallogr., Sect. A: Found. Crystallogr.* **2008**, *64*, 112−122.
(63) Dolomanov, O. V.; Bourhis, L. J.; Gildea, R. J.; Howard, J. A. K.; Puschmann, H. $OLEX^2$: a complete structure solution, refinement and analysis program. *J. Appl. Crystallogr.* **2009**, *42*, 339−341.
(64) Spackman, M. A.; McKinnon, J. J. Fingerprinting intermolecular interactions in molecular crystals. *CrystEngComm* **2002**, *4*, 378−392.
(65) Kupcewicz, B.; Małecka, M. Role of Crystal Packing and Weak Intermolecular Interactions in the Solid State Fluorescence of N-Methylpyrazoline Derivatives. *Cryst. Growth Des.* **2015**, *15*, 3893−3904.

https://doi.org/10.1021/acsomega.2c03047
ACS Omega 2022, 7, 24838−24850